Low-Temperature-Processed Colloidal Quantum Dots as Building Blocks for Thermoelectrics

Mohamad I. Nugraha, Hyunho Kim, Bin Sun, Md Azimul Haque,
Francisco Pelayo Garcia de Arquer, Diego Rosas Villalva, Abdulrahman El-Labban,
Edward H. Sargent, Husam N. Alshareef, and Derya Baran*

Colloidal quantum dots (CQDs) are demonstrated to be promising materials to realize high-performance thermoelectrics owing to their low thermal conductivity. The most studied CQD films, however, are using long ligands that require high processing and operation temperature (>400 °C) to achieve optimum thermoelectric performance. Here the thermoelectric properties of CQD films cross-linked using short ligands that allow strong inter-QD coupling are reported. Using the ligands, p-type thermoelectric solids are demonstrated with a high Seebeck coefficient and power factor of 400 µV K^{-1} and 30 µW m^{-1} K^{-2}, respectively, leading to maximum ZT of 0.02 at a lower measurement temperature (<400 K) and lower processing temperature (<300 °C). These ligands further reduce the annealing temperature to 175 °C, significantly increasing the Seebeck coefficient of the CQD films to 580 µV K^{-1}. This high Seebeck coefficient with a superior ZT near room temperature compared to previously reported high temperature-annealed CQD films is ascribed to the smaller grain size, which enables the retainment of quantum confinement and significantly increases the hole effective mass in the films. This study provides a pathway to approach quantum confinement for achieving a high Seebeck coefficient yet strong inter-QD coupling, which offers a step toward low-temperature-processed high-performance thermoelectric generators.

Thermoelectric materials are of interest because of their ability to convert heat into electricity. The performance of thermoelectric materials is characterized by a dimensionless figure of merit, $ZT = \sigma S^2 T/\kappa$, where σ, S, κ, and T are electrical conductivity, Seebeck coefficient, thermal conductivity, and temperature, respectively. Nanostructured materials are promising thermoelectrics because they offer a large number of grain boundaries in the films, a feature that is expected to promote phonon scattering, thus lowering thermal conductivity compared to their bulk counterparts.[1,2] At the same time, quantum confinement of charge carriers leads to sharp density of states (DOS) that increases the energy dependence of the DOS near the Fermi level. This system, with its rapid change in the DOS near the Fermi level, meets a key requirement for achieving a high Seebeck coefficient.[3–6]

Colloidal quantum dots (CQDs) are an intensively studied nanostructured system that have been advanced as semiconducting building blocks in optoelectronic devices.[7–10] Ease of solution-processing of these materials allows the fabrication of electronic devices using low-cost scalable processes, such as coating and printing methods.[11–14] CQDs have a well-established synthesis that provides precise control of their shape and size with bandgap tunable from the visible to the infrared regions, making them of interests for thermoelectrics.[15,16] Studies of CQDs for thermoelectrics,[14,15] include recent work by Ding et al. have reported thermoelectric thin films based on lead chalcogenide CQDs displaying promising thermoelectric performance (Seebeck coefficient of 290 µV K^{-1}).[17] Ibanez et al. demonstrated a system treated at high temperature and pressure that exhibits excellent thermoelectric performance.[18–20] Despite these encouraging results, the most studied CQD films have been using long ligands that require high processing and operation temperature (>400 °C) to achieve optimum thermoelectric performance. It is of interest to design CQD systems to achieve optimum thermoelectric performance with lower processing temperatures by employing shorter molecular ligands that allow strong QD coupling. This

Dr. M. I. Nugraha, M. A. Haque, D. R. Villalva, Dr. A. El-Labban,
Prof. D. Baran
King Abdullah University of Science and Technology (KAUST)
Physical Sciences and Engineering Division (PSE)
KAUST Solar Center (KSC)
Thuwal 23955-6900, Saudi Arabia
E-mail: derya.baran@kaust.edu.sa
H. Kim, Prof. H. N. Alshareef
King Abdullah University of Science and Technology (KAUST)
Physical Sciences and Engineering Division (PSE)
Thuwal 23955-6900, Saudi Arabia
Dr. B. Sun, Dr. F. P. G. de Arquer, Prof. E. H. Sargent
Department of Electrical and Computer Engineering
University of Toronto
Toronto, Ontario M5S 3G4, Canada

ADVANCED
SCIENCE NEWS
www.advancedsciencenews.com

ADVANCED
ENERGY
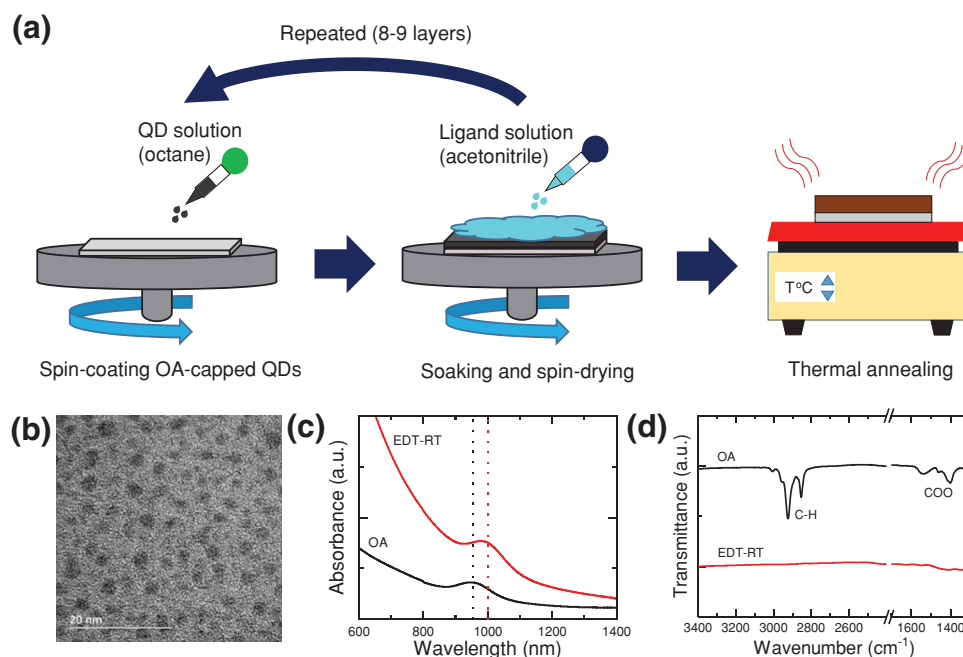**MATERIALS**
www.advenergymat.de

Figure 1. a) Schematic of a PbS CQD film deposition procedure, b) TEM image of OA-stabilized PbS CQDs, c) absorption, and d) FTIR spectra of PbS CQD films with OA and EDT ligands.

approach is expected to retain quantum confinement, which is predicted to yield a higher ZT at room temperature (RT).[6,21–23] This would open the door to the realization of power sources for low-power consuming microsensors and microelectronic devices.

In this work, we investigate solution-processed CQD film thermoelectrics using short thiol-based ligands. With these ligands, we obtain p-type thermoelectrics that exhibit Seebeck coefficients and power factors as high as 400 µV K^{-1} and 30 µW m^{-1} K^{-2}, leading to a maximum ZT value of 0.02 at a relatively low operation temperature (<400 K). We found that reducing the annealing temperature to 175 °C allows us to achieve a Seebeck coefficient as high as 580 µV K^{-1}. Analysis on grain size and hole effective mass supported by Hall Effect measurement account for an increased Seebeck coefficient in low temperature-annealed CQD films.

The deposition of CQD films was performed employing a layer-by-layer (LbL) spin-casting method (**Figure 1**a). In CQD inks, long alkyl chain organic molecules (oleic acid/OA) are used as one means to control the size of the CQDs during synthesis and to provide stable QD colloids in most organic solvents. In this study, we used lead sulfide (PbS) CQDs because of their remarkable properties as semiconducting building blocks particularly for highly efficient optoelectronics.[24–27] We spin-coated OA-PbS CQD dispersion from a nonpolar medium (octane) on clean glass substrates. Interdots charge transport is in this configuration precluded by the presence of OA long-chain barriers. We then carried out a solid-state exchange to replace the long ligands with short ligands, thus enhancing the electronic properties of the CQD films.[28,29] Here we used short 1,2 ethanedithiol (EDT) ligands that, with two symmetric thiol groups, lead to cross-linked CQDs exhibiting charge transport.[30] The exchange of OA ligands with EDT results in

nonsoluble CQD films, which allows us to build CQD layers using LbLs. The deposition of the ensuing layers is important to achieve uniform CQD films and to get desired film thickness. With nine consecutive LbL steps, we obtained 200 nm thick crack-free CQD films (Figure S1, Supporting Information). We then employed a final annealing step to control the presence of the remaining organic ligands and solvents and to promote stronger coupling between CQDs (Figure 1a). Figure 1b provides a transmission electron microscopy (TEM) image of OA-PbS QDs with a diameter of 3 nm. These OA-capped CQDs demonstrate an excitonic peak in the absorption spectra around 941 nm (1.3 eV). After ligand exchange with EDT, a red-shift in the absorption spectra is observed (Figure 1c), indicative of decreased inter-CQD distance and exciton spill over. The success of the ligand exchange was confirmed by Fourier transform infrared spectroscopy (FTIR) where C–H and COO stretching around 2900 and 1500 cm^{-1} vanish (Figure 1d).

We first measured the electrical conductivity of the 300 °C annealed PbS CQD films (EDT-QD-300) as a function of temperature ($T_{measure}$) as illustrated in **Figure 2**a. The electrical conductivity increases with increasing $T_{measure}$, which indicates typical thermally activated transport mechanism (see Figure S2 in the Supporting Information for detailed fitting of temperature-dependent conductivity). This indicates that the electrical network of CQD film contains energy barriers to overcome, most likely at the grain/domain boundaries, which are also beneficial for phonon scattering resulting in lower thermal conductivity than of that in bulk materials (see Figure S3 in the Supporting Information for the measured thermal conductivity). The measured electrical conductivity in the EDT-QD-300 films is higher than that in previously reported ethylenediamine-capped CQD thermoelectric films (<0.4 S cm^{-1}); the latter of which were annealed at 400 °C.[17] This indicates
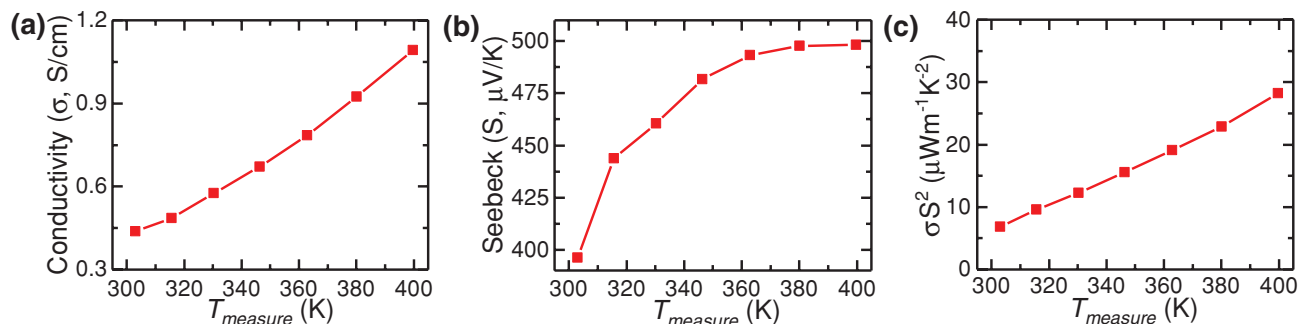
Figure 2. a) Temperature-dependent electrical conductivity, b) Seebeck coefficient, and c) power factor of EDT-QD-300 films.

that EDT passivation provides stronger coupling between QDs than the ethylenediamine ligand as well as a lower annealing temperature up to 300 °C. Figure 2b presents the Seebeck coefficient of our EDT-QD-300 films as a function of $T_{measure}$. The positive sign of the Seebeck coefficient shows that the cross-linking of the PbS CQD films with EDT ligands provides p-type thermoelectric behavior. This is in line with previously reported EDT-capped PbS CQD field-effect transistors demonstrating holes as the majority carrier type.[31] The hole concentration in the films has been reported to increase upon air exposure, leading to an increased p-type doping.[32] The EDT-QD-300 films exhibit a Seebeck coefficient of 400 µV K^{-1} at RT. This remarkable Seebeck coefficient is significantly higher than that of bulk PbS (≈100 µV K^{-1}), which is enabled by a large number of grain boundaries in CQD films leading to slightly larger bandgap than bulk.[33] The power factor (σS^2) values as a function of $T_{measure}$ are calculated and presented for EDT-QD-300 films in Figure 2c. Similar to electrical conductivity and Seebeck coefficient, the power factor increases with increasing $T_{measure}$ up to 30 µW m^{-1} K^{-2}, leading to maximum ZT value of 0.02 at relatively low operation temperatures (<400 K). This ZT value near RT operation is also superior to previously reported PbS CQD thermoelectrics (ZT near RT<10^{-3}) which were also annealed at high temperatures (>400 °C).[17,18]

We then varied the annealing temperature (T_{anneal}) of the PbS CQD films to further explore the thermoelectric properties of the CQD solids, particularly with lower T_{anneal}. Similar to the EDT-QD-300, we did not observe any C–H or COO stretching around 2900 and 1500 cm^{-1} from OA ligands in the FTIR spectra of EDT-cross-linked PbS CQD films with different T_{anneal} (Figure S4, Supporting Information). It is also clear that the typical bond stretching has vanished even in the unannealed EDT-cross-linked films, which indicates that the removal of the OA at higher T_{anneal} is mainly due to an effective ligand exchange (LE) reaction, however, not as a result of thermal decomposition of OA ligands. In addition, X-ray diffraction (XRD) analysis illustrated in Figure S5 in the Supporting Information also revealed that the higher annealing temperature did not induce any new phases in the CQD films and resulted in enhanced crystallinity based on the increased XRD peak intensities. We then analyzed thermoelectric properties of EDT-QD-175, EDT-QD-200, EDT-QD-250, and EDT-QD-300 films. We first observed that the electrical conductivity in the CQD films increases with increasing T_{anneal} as displayed in **Figure 3**a. On

the other hand, the electrical conductivity was also found to increase with increasing $T_{measure}$.[34] To understand the charge conduction mechanism in the films, we did fitting in the logarithmic plot of the conductivity as a function of reciprocal $T_{measure}$ (Figure S2, Supporting Information). From the fitting results, the conduction mechanism follows thermally activated transport behavior with different activation energy. As presented in Figure 3b, the activation energy was found to be the smallest in EDT-QD-300, indicating an improved charge transport scenario due to a reduced inter-QD barrier height and distance for films annealed at a higher temperature.

The Seebeck coefficient in the CQD films with different T_{anneal} is presented in Figure 3c. We found that the Seebeck coefficient significantly increases when the films are treated with lower T_{anneal}. In EDT-QD-175 films, the measured Seebeck coefficient increases to 580 µV K^{-1} at RT. This is the highest value reported for low temperature-annealed PbS CQDs based thermoelectric films at RT to date. Interestingly, the measured Seebeck coefficient for EDT-QD-175 demonstrates negligible dependence on $T_{measure}$ suggesting a more quantum confined nature. Figure 3d presents the power factor of the EDT-cross-linked PbS CQD films treated with different T_{anneal}. EDT-QD-300 films have a higher power factor compared to lower processing temperatures (e.g., EDT-QD-175) as a result of their higher conductivity. In EDT-QD-175 films, the conductivity drop stems from a more confined nature of the films, which leads to the lower measured power factor, even though the Seebeck coefficient is high. Nevertheless, the measured power factor (5 µW m^{-1} K^{-2}) in EDT-QD-175 films is still comparable with previously reported PbS CQD-based thermoelectrics (5.6 µW m^{-1} K^{-2} with 400 °C annealing).[17] Furthermore, these CQD films with high Seebeck coefficients along with significantly lower temperature processing will be potentially effective thermoelectric materials when they are blended with highly conductive matrix materials.

To study the morphology of the CQD films with different T_{anneal}, we performed scanning electron microscopy (SEM) measurements. **Figure 4**a–d provide SEM images of EDT-cross-linked PbS CQD films treated with different T_{anneal} (from EDT-QD-175 to EDT-QD-300). As expected, CQD films demonstrate less sintering effect for lower T_{anneal}, leading to smaller grain sizes in the films. This smaller grain size is also confirmed in the atomic force microscopy (AFM) images of the CQD films after treatment with lower T_{anneal} as displayed in Figure 4e–h. The grain size for EDT-QD-175 films is ≈8.8 nm, while

**ADVANCED
SCIENCE NEWS**

www.advancedsciencenews.com
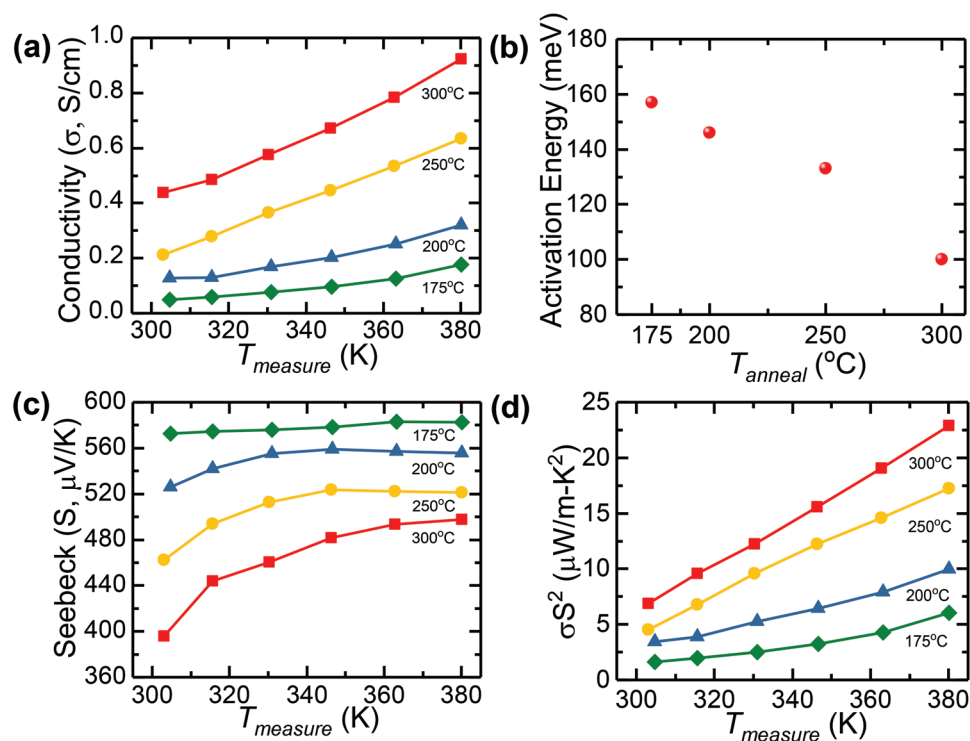
**ADVANCED
ENERGY
MATERIALS**

www.advenergymat.de

Figure 3. a) Temperature-dependent electrical conductivity in EDT-QD-175 (green), EDT-QD-200 (blue), EDT-QD-250 (yellow), and EDT-QD-300 films (red), b) activation energy in PbS CQD films with different T_{anneal}; c) Temperature-dependent Seebeck coefficient and d) power factor of EDT-cross-linked PbS CQD films with different T_{anneal}.

significantly larger grain sizes of ≈45 nm are observed for EDT-QD-300 films. More details on the average grain size in the CQD films with different T_{anneal} are given in Figures S6 and S7 in the Supporting Information. The small grain size results in a greater number of grain boundaries and less film crystallinity that can promote phonon scattering, thus reducing thermal conductivity in the films (Figures S3 and S5, Supporting Information). Furthermore, the grain size in EDT-QD-175 films is smaller than the Bohr exciton radius of PbS (≈20 nm), which indicates that the films are approaching the quantum confinement regime.

Traditionally, a trade-off exists between electrical conductivity and the Seebeck coefficient. An increase of the former is accompanied by the decrease of the latter (or vice versa), leading to a limited power factor.[35–38] However, we observe that both the electrical conductivity and the Seebeck coefficient increase simultaneously as a function of $T_{measure}$ (Figure 2a,b), which is not typical classical thermoelectric behavior. To understand this phenomenon, we performed the Hall Effect measurement to estimate the hole mobility (μ_h) and carrier density (p) in the films. The Hall voltage dependence on the magnetic field
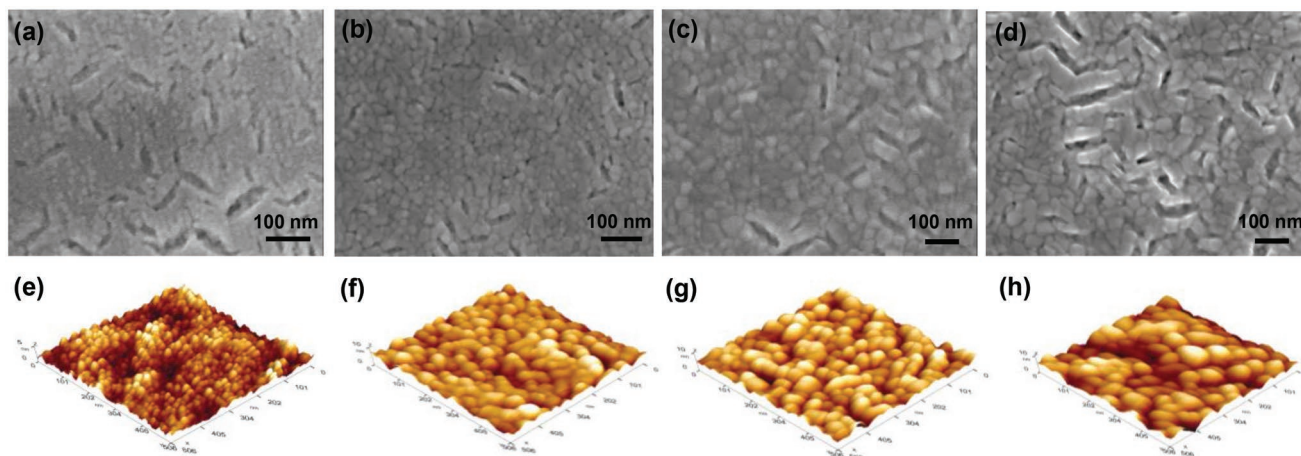

Figure 4. SEM and AFM images of a,e) EDT-QD-175, b,f) EDT-QD-200, c,g) EDT-QD-250, and d,h) EDT-QD-300 films.
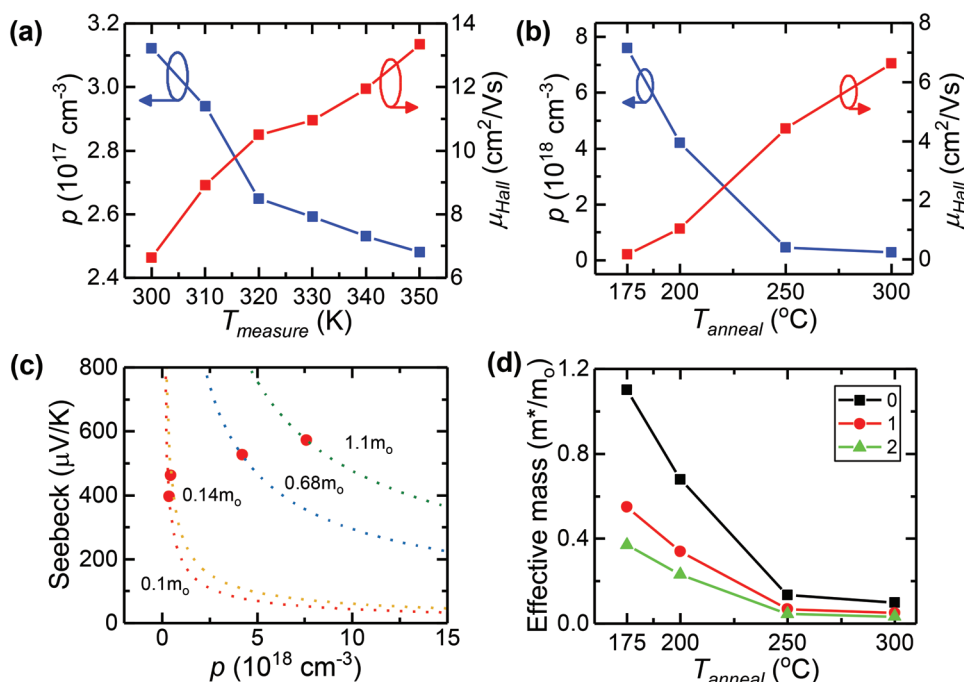
Figure 5. a) Temperature-dependent carrier density and Hall mobility in EDT-QD-300 films, b) room temperature carrier density and Hall mobility in PbS CQD films with different T_{anneal}; c) Hole effective mass in EDT-QD-175 (green), EDT-QD-200 (blue), EDT-QD-250 (yellow), and EDT-QD-300 (red) films estimated from Pisarenko plot; d) Hole effective mass by considering different scattering parameter.

indicates a p-type behavior, which agrees with the sign of See-beck coefficient measurement results (Figure S8, Supporting Information). The μ_h and p for EDT-QD-300 are displayed in **Figure 5**a. The increased Hall mobility with increasing $T_{measure}$ agrees with the previously explained conductivity trends and supports thermally activated transport behavior in the PbS CQD films cross-linked with EDT ligands. The carrier density, on the other hand, shows the opposite trend where carrier density decreases with increasing $T_{measure}$. According to Pisarenko equation, the change in carrier density can influence the Seebeck coefficient (S) as follows

$$S = \frac{8\pi^2 k_B^2}{3eh^2} m^* T \left(\frac{\pi}{3p}\right)^{\frac{2}{3}} (r+1) \qquad (1)$$

where T, k_B, e, h, m^*, and r are $T_{measure}$, Boltzmann constant, charge constant, Planck constant, effective mass, and scattering parameter respectively. The Seebeck coefficient is inversely proportional to carrier density (p), while it increases with increasing $T_{measure}$ and the effective mass in the materials. In p-type materials, the Seebeck coefficient is known to be proportional to the offset between Fermi level and valence band ($\langle E_F - E_V \rangle$). The decrease of carrier density indicates that the Fermi level of the materials moves further away from the transport level (valence band for p-type; conduction band for n-type), which leads to an increased Fermi level and valence/conduction band offset ($\langle E_F - E_V \rangle$) ultimately resulting in a higher Seebeck coefficient.[39,40] The increase of the Seebeck coefficient as a function of the effective mass and $T_{measure}$ in Equation (1) arises from a higher DOS available indicating a greater probability for charge

carriers to be excited to a higher energy level when a temperature gradient is applied to the material. Figure 5a presents Hall Effect carrier density for EDT-QD-300 films as a function of $T_{measure}$. The higher carrier density in the EDT-QD-300 films at lower $T_{measure}$ indicates that the Fermi level is located near a valence band resulting in a smaller $\langle E_F - E_V \rangle$, hence a lower Seebeck coefficient. When $T_{measure}$ is increased, we observe a lower carrier density suggesting a shift of the Fermi level toward the conduction band, which leads to an increase of the Seebeck coefficient. This result can be explained by temperature-dependent Fermi level relationship in p-type semiconductors ($E_F = E_V + k_b T \ln(N_V/N_A)$), where N_V and N_A are effective DOS in a valence band and concentration of acceptors (holes), respectively. In addition, some minority charge carriers (electrons) might also be activated at higher $T_{measure}$ due to certain level of ambipolarity in PbS CQD films, which can contribute to the Fermi level rising toward the conduction band.[8,31,32] This condition results in an increase of $\langle E_F - E_V \rangle$ offset leading to a larger Seebeck coefficient in the CQD films with increasing $T_{measure}$.

The Hall Effect measurement was also performed in PbS CQD films treated with different T_{anneal} (EDT-QD-175, EDT-QD-200, EDT-QD-250, and EDT-QD-300). Figure 5b illustrates the increased Hall mobility with increasing T_{anneal} that can explain the increased conductivity in the CQD films treated with higher T_{anneal}. On the other hand, the carrier density was found to increase with decreasing T_{anneal}. The highest carrier density was measured in EDT-QD-175 films that exhibit the highest Seebeck coefficient. This behavior contrasts with the relationship in the Pisarenko Equation (1), where higher Seebeck coefficients are commonly associated with lower charge carrier concentrations. As we refer to Equation (1), we associate

ADVANCED
SCIENCE NEWS
www.advancedsciencenews.com

ADVANCED
ENERGY
MATERIALS
www.advenergymat.de

this result to the change in the hole effective mass that may play an important role in determining the measured Seebeck coefficient. To challenge this argument, we estimated the hole effective mass by fitting the measured Seebeck coefficient versus Hall carrier density results to the Pisarenko equation. The fitting results that are presented in Figure 5c show the increased effective mass with decreasing T_{anneal} (see Figure S9 in the Supporting Information for the detailed fitting). The estimated hole effective mass in EDT-QD-300 films is $0.1m_o$, and it increases up to $1.1m_o$ in EDT-QD-175 films. This one order of magnitude increase of the hole effective mass is the microscopic origin of the higher Seebeck coefficient in the films with lower T_{anneal}, even though at the same time the carrier density is increased. The increased effective mass corresponds to a higher DOS providing more probability for holes to excite to higher energy while one side of the films is heated. Furthermore, the higher DOS also indicates that the lower T_{anneal} films (EDT-QD-175 and EDT-QD-200) are approaching the quantum confinement regime, which is also supported by the fact that the measured grain size (Figure S6, Supporting Information) is quite close to the Bohr exciton radius of PbS ($\approx$20 nm).[41]

Finally, it is important to note that the hole effective mass in Figure 5c was estimated using a scattering parameter ($r = 0$) in the Pisarenko equation that assumes the contribution of acoustic phonon scattering in the CQD films. We also consider other contributions that may come from an optical phonon ($r = 1$) and ionized impurity scattering ($r = 2$). Figure 5d presents the hole effective mass in EDT-cross-linked CQD films by employing different scattering parameters. The ionized impurity scattering contribution that results in the lowest measured effective mass can be excluded from our assumptions since it is dominant at a very low measurement temperature.[42] Meanwhile, the contribution from optical phonon scattering is considerable when dealing with high temperatures. Since our thermoelectric measurement was performed at moderate temperature (<400 K), we believe that acoustic phonon scattering makes a more dominant contribution in our CQD films. Therefore, the estimated effective mass presented in Figure 5c is valid in our materials.

In conclusion, we have demonstrated high-performance p-type thermoelectric materials based on PbS CQDs cross-linked with EDT ligands. The EDT-cross-linked PbS CQD films show Seebeck coefficients of 400 μV K^{-1} and power factors of 30 μW m^{-1} K^{-2} leading to a ZT value of 0.02 near RT, which is superior to previously reported high temperature-annealed CQD films. When we reduce the annealing temperature, a remarkable enhancement of the Seebeck coefficient to 580 μV K^{-1} was observed, which is the highest value reported for low temperature-annealed PbS CQDs based thermoelectric films at RT. We found that the interplay between grain size, carrier density, and effective mass is the fundamental origin of the increased Seebeck coefficient in films treated with lower annealing temperatures. This comprehensive study, providing a pathway to approach quantum confinement for achieving a high Seebeck coefficient, would be promising for the realization of low-temperature-processed high output thermal voltage nanogenerators constructed from CQD systems in the future.

Experimental Section

Preparation of PbS QDs: CQDs were synthesized following previously reported methods.[15] Bis(trimethylsilyl) sulfide (TMS, synthesis grade) (0.18 g, 1 mol) was added to 1-octadecene (ODE) (10 mL) that had been dried and degassed by heating to 80 °C under a vacuum for 24 h. A mixture of OA (1.34 g, 4.8 mmol), PbO (0.45 g, 2.0 mmol), and ODE (14.2 g, 56.2 mmol) was heated to 95 °C under a vacuum for 16 h and placed under Ar. The flask temperature was increased to 120 °C and the TMS/ODE mixture was injected. After injection, the flask was allowed to cool gradually to 35 °C. The CQDs were precipitated using distilled acetone (50 mL) and centrifuged. The supernatant was discarded and the precipitate redispersed in toluene. The CQDs were precipitated again using methanol (20 mL), centrifuged (5 min), dried, dispersed in octane (50 mg mL^{-1}) and transported into a nitrogen glovebox (oxygen below 2 ppm and moisture below 10 ppm).

Deposition of PbS CQD Films: Glass substrates were ultrasonically cleaned with acetone and isopropanol for 5 min, respectively. After drying at 140 °C for 10 min, the substrates were treated in a UV ozone chamber for 15 min. The solution of oleic acid-stabilized PbS CQDs in octane (50 mg mL^{-1}) was spin-coated on the cleaned glass substrates at 2500 rpm for 60 s. To improve charge transport within CQD films, the long OA ligands were exchanged with EDT. The concentration of the EDT ligands was 1% v/v in acetonitrile. The LE process was done by dropping the ligand solution on the CQD films for 30 s and then spin-drying the solution at 2500 rpm for 60 s. After each LE, pure acetonitrile was dropped to remove the exchanged native oleic acid ligands. The CQD film deposition and the LE process were repeated nine times to reach the desired thickness. Finally, the EDT-cross-linked CQD films were annealed on a hot plate at different temperatures for 30 min. All processes were performed in an N$_2$-filled glove box.

Film Characterization: The optical absorption spectra of PbS CQD films deposited on glass substrates were measured by using a Cary 5000 UV–vis spectrometer (Agilent Technologies). The FTIR measurements were done on the films deposited on glass substrates using Cary 680 with the attenuated total reflectance mode in the air. The film thickness ($\approx$200 nm) was measured using a Tencor profilometer. The morphology of the CQD films was measured using atomic force microscopy (Solver Next SPM from NT-MDT) and SEM (Carl Zeiss Auriga).

The charge carrier mobility and carrier concentration in the films (1 cm × 1 cm on glass) were measured using Hall Effect measurement system (Lake Shore 7700A) with the van der Pauw configuration. The measurement was done in temperature range of 300–350 K (step of 10 K) under a magnetic field of 10 kG.

Thermoelectric Characteristic Measurement: Electrical conductivity and Seebeck coefficient were measured by the linear four-probe and temperature differential methods, respectively. The measurement was done using a thermoelectric characterization setup RZ2001i (Ozawa Science Co. Ltd., Japan) under continuous flow of Ar/H$_2$ gas. The thermal conductivity of the CQD thin films was measured by using Linseis Thin Film Analysis (TFA) under a vacuum. The details for electrical conductivity, Seebeck coefficient, and thermal conductivity measurements are given in the Supporting Information.

Supporting Information

Supporting Information is available from the Wiley Online Library or from the author.

Acknowledgements

Conflict of Interest

The authors declare no conflict of interest.

Keywords

[1] J. J. Urban, *Nat. Nanotechnol.* **2015**, *10*, 997.

[2] J. D. Forster, J. J. Lynch, N. E. Coates, J. Liu, H. Jang, E. Zaia, M. P. Gordon, M. Szybowski, A. Sahu, D. G. Cahill, J. J. Urban, *Sci. Rep.* **2017**, *7*, 1.

[3] R. Y. Wang, J. P. Feser, J. S. Lee, D. V. Talapin, R. Segalman, A. Majumdar, *Nano Lett.* **2008**, *8*, 2283.

[4] N. Xu, Y. Xu, J. Zhu, *npj Quantum Mater.* **2017**, *2*, 51.

[5] J. Zhou, R. Yang, *Phys. Rev. B* **2010**, *82*, 075324.

[6] J. Mao, Z. Liu, Z. Ren, *npj Quantum Mater.* **2016**, *1*, 16028.

[7] A. H. Ip, S. M. Thon, S. Hoogland, O. Voznyy, D. Zhitomirsky, R. Debnath, L. Levina, L. R. Rollny, G. H. Carey, A. Fischer, K. W. Kemp, I. J. Kramer, Z. Ning, A. J. Labelle, K. W. Chou, A. Amassian, E. H. Sargent, *Nat. Nanotechnol.* **2012**, *7*, 577.

[8] M. I. Nugraha, R. Häusermann, S. Z. Bisri, H. Matsui, M. Sytnyk, W. Heiss, J. Takeya, M. A. Loi, *Adv. Mater.* **2015**, *27*, 2107.

[9] D. Zhitomirsky, M. Furukawa, J. Tang, P. Stadler, S. Hoogland, O. Voznyy, H. Liu, E. H. Sargent, *Adv. Mater.* **2012**, *24*, 6181.

[10] L.-H. Lai, W. Gomulya, L. Protesescu, M. V. Kovalenko, M. A. Loi, *Phys. Chem. Chem. Phys.* **2014**, *16*, 7531.

[11] I. J. Kramer, J. C. Minor, G. Moreno-Bautista, L. Rollny, P. Kanjanaboos, D. Kopilovic, S. M. Thon, G. H. Carey, K. W. Chou, D. Zhitomirsky, A. Amassian, E. H. Sargent, *Adv. Mater.* **2015**, *27*, 116.

[12] M. I. Nugraha, R. Häusermann, S. Watanabe, H. Matsui, M. Sytnyk, W. Heiss, J. Takeya, M. A. Loi, *ACS Appl. Mater. Interfaces* **2017**, *9*, 4719.

[13] A. G. Shulga, L. Piveteau, S. Z. Bisri, M. V. Kovalenko, M. A. Loi, *Adv. Electron. Mater.* **2016**, *2*, 1500467.

[14] D. M. Balazs, D. N. Dirin, H.-H. Fang, L. Protesescu, G. H. ten Brink, B. J. Kooi, M. V. Kovalenko, M. A. Loi, *ACS Nano* **2015**, *9*, 11951.

[15] M. A. Hines, G. D. Scholes, *Adv. Mater.* **2003**, *15*, 1844.

[16] D. V. Talapin, J.-S. Lee, M. V. Kovalenko, E. V. Shevchenko, *Chem. Rev.* **2010**, *110*, 389.

[17] D. Ding, D. Wang, M. Zhao, J. Lv, H. Jiang, C. Lu, Z. Tang, *Adv. Mater.* **2017**, *29*, 1603444.

[18] M. Ibáñez, Z. Luo, A. Genç, L. Piveteau, S. Ortega, D. Cadavid, O. Dobrozhan, Y. Liu, M. Nachtegaal, M. Zebarjadi, J. Arbiol, M. V. Kovalenko, A. Cabot, *Nat. Commun.* **2016**, *7*, 1.

[19] M. Ibáñez, R. Zamani, S. Gorsse, J. Fan, S. Ortega, D. Cadavid, J. R. Morante, J. Arbiol, A. Cabot, *ACS Nano* **2013**, *7*, 2573.

[20] S. Ortega, M. Ibáñez, Y. Liu, Y. Zhang, M. V. Kovalenko, D. Cadavid, A. Cabot, *Chem. Soc. Rev.* **2017**, *46*, 3510.

[21] T. E. Humphrey, H. Linke, *Phys. Rev. Lett.* **2005**, *94*, 3.

[22] I. D. Hicks, M. S. Dresselhaus, *Phys. Rev. B* **1993**, *47*, 8.

[23] L. D. Hicks, M. S. Dresselhaus, *Phys. Rev. B* **1993**, *47*, 727.

[24] J. Xu, O. Voznyy, M. Liu, A. R. Kirmani, G. Walters, R. Munir, M. Abdelsamie, A. H. Proppe, A. Sarkar, F. P. García De Arquer, M. Wei, B. Sun, M. Liu, O. Ouellette, R. Quintero-Bermudez, J. Li, J. Fan, L. Quan, P. Todorovic, H. Tan, S. Hoogland, S. O. Kelley, M. Stefik, A. Amassian, E. H. Sargent, *Nat. Nanotechnol.* **2018**, *13*, 456.

[25] A. R. Kirmani, A. D. Sheikh, M. R. Niazi, M. A. Haque, M. Liu, F. P. G. de Arquer, J. Xu, B. Sun, O. Voznyy, N. Gasparini, D. Baran, T. Wu, E. H. Sargent, A. Amassian, *Adv. Mater.* **2018**, *1801661*, 1.

[26] Z. Ning, X. Gong, R. Comin, G. Walters, F. Fan, O. Voznyy, E. Yassitepe, A. Buin, S. Hoogland, E. H. Sargent, *Nature* **2015**, *523*, 324.

[27] Y. Cao, A. Stavrinadis, T. Lasanta, D. So, G. Konstantatos, *Nat. Energy* **2016**, *1*, 16035.

[28] G. H. Carey, L. Levina, R. Comin, O. Voznyy, E. H. Sargent, *Adv. Mater.* **2015**, *27*, 3325.

[29] C. R. Kagan, C. B. Murray, *Nat. Nanotechnol.* **2015**, *10*, 1013.

[30] M. I. Nugraha, H. Matsui, S. Watanabe, T. Kubo, R. Häusermann, S. Z. Bisri, M. Sytnyk, W. Heiss, M. A. Loi, J. Takeya, *Adv. Electron. Mater.* **2017**, *3*, 1600360.

[31] M. I. Nugraha, S. Kumagai, S. Watanabe, M. Sytnyk, W. Heiss, M. A. Loi, J. Takeya, *ACS Appl. Mater. Interfaces* **2017**, *9*, 18039.

[32] D. M. Balazs, M. I. Nugraha, S. Z. Bisri, M. Sytnyk, W. Heiss, M. A. Loi, *Appl. Phys. Lett.* **2014**, *104*, 112104.

[33] E. I. Rogacheva, I. M. Krivulkin, O. N. Nashchekina, A. Y. Sipatov, V. V. Volobuev, M. S. Dresselhaus, *Appl. Phys. Lett.* **2001**, *78*, 1661.

[34] D. K. Kim, Y. Lai, T. R. Vemulkar, C. R. Kagan, *ACS Nano* **2011**, *5*, 10074.

[35] Z. Fan, P. Li, D. Du, J. Ouyang, *Adv. Energy Mater.* **2017**, *7*, 1602116.

[36] K. F. Hsu, *Science* **2004**, *303*, 818.

[37] S. K. Mishra, S. Satpathy, O. Jepsen, *J. Phys.: Condens. Matter* **1997**, *9*, 461.

[38] O. Bubnova, Z. U. Khan, A. Malti, S. Braun, M. Fahlman, M. Berggren, X. Crispin, *Nat. Mater.* **2011**, *10*, 429.

[39] I. M. Vitomirov, G. D. Waddill, C. M. Aldao, S. G. Anderson, C. Capasso, J. H. Weaver, *Phys. Rev. B* **1989**, *40*, 3483.

[40] W. Zhou, J. Vavro, N. M. Nemes, J. E. Fischer, F. Borondics, K. Kamarás, D. B. Tanner, *Phys. Rev. B* **2005**, *71*, 205423.

[41] W. Koh, S. R. Saudari, A. T. Fafarman, C. R. Kagan, C. B. Murray, *Nano Lett.* **2011**, *11*, 4764.

[42] Y. I. Ravich, B. A. Efimova, V. I. Tamarchenko, *Phys. Status Solidi B* **1971**, *43*, 11.